Tuning Ionic Screening to Accelerate Electrochemical CO_2 Reduction in Ionic Liquid Electrolytes

Beichen Liu,[†] Wenxiao Guo,[†] and Matthew A. Gebbie[†]*

[†]Department of Chemical and Biological Engineering, University of Wisconsin–Madison, Madison, Wisconsin 53706, United States

Keywords: *Electrocatalysis, ionic liquids, electric double layer, interfaces, electrochemistry*

*Address correspondence to gebbie@wisc.edu

Abstract

Electric double layer formation often governs the rate and selectivity of CO_2 electrochemical reduction. Ionic correlations critically define double layer properties that are essential to electrocatalytic performance, including capacitance and localization of potential gradients. However, the influence of ionic correlations on CO_2 electro-reduction remains unexplored. Here, we use electrochemical conversion of CO_2 to CO in ionic liquid-based electrolytes to investigate how the emergence of ionic correlations with increasing ion concentration influences reaction rates and selectivity. Remarkably, we find substantial acceleration of potential-dependent CO_2 reduction rates and notable enhancement of faradaic efficiency to CO at intermediate concentrations of 0.9 M ionic liquid in acetonitrile, a concentration regime that has not been studied previously. We find that onset potentials for CO_2 reduction remain relatively unchanged at -2.01 V vs. Ag/Ag^+ from 0.025 M up to 1.1 M and increase to -2.04 V vs. Ag/Ag^+ in the limit of neat ionic liquids. Hence, the acceleration of CO_2 reduction we observe originates from the amplification of potential-dependent driving forces, as opposed to changes in onset potential. Importantly, our findings are general across co-catalytic and non-catalytic ions. We propose that concentrations of maximum reactivity correspond to conditions where electric double layers exhibit the strongest screening, which would localize electric fields to stabilize polar intermediates. Our study demonstrates that tuning bulk electrostatic screening lengths via modulation of ionic clustering provides a general approach to accelerating both inner sphere and outer sphere electrochemical reactions.

Introduction

Electrochemical reduction of CO_2 to CO and other products could provide opportunities to minimize the carbon footprints of industrial processes by replacing fossil fuels with waste or atmospheric CO_2. Conversion of CO_2 proceeds via mechanisms where the first step often involves a two proton, two-electron half-reaction to convert CO_2 into CO (Eq. 1), usually through the formation of a negative radical intermediate, [1, 2] which can then further react to wide-ranging products. Notably, the concurrent generation of H_2 by the hydrogen evolution reaction (HER) also occurs via a two proton, two-electron half-reaction at similar, often lower, onset potentials, particularly in aqueous solutions. Hence, a key challenge for the implementation of electrochemical CO_2 reduction is to devise approaches to favor CO_2 reduction, while simultaneously inhibiting electron flow into the HER pathway.

$$CO_2 + 2H^+ + 2e^- \rightarrow CO + H_2O \quad (1)$$

Recently, chemical modulation of electrolyte properties, such as the inclusion of cations that stabilize CO_2 reduction transition states, has emerged as an important tool in tipping the balance away from HER and towards CO_2 reduction. [3-7] For example, ionic liquid-based electrolytes where cations are designed to selectively coordinate CO_2 have emerged as promising co-catalytic promoters of selective electro-reduction of CO_2 to CO. [3, 6-10]

Ionic liquids are salts typically composed of bulky organic cations combined with a variety of anions, which may be organic or inorganic. [11-13] While neat ionic liquids exhibit advantageous properties for CO_2 electro-reduction, including high electrochemical stability, CO_2 solubility, and intrinsic ionic conductivity, they are too viscous to facilitate high current densities needed for practical processes. As a result, ionic liquids are often blended into aqueous and non-aqueous solutions when implemented in electrocatalytic studies.

Co-catalysis of CO_2 reduction via ionic liquids was first demonstrated by Rosen and coworkers, where aqueous electrolytes with ion concentrations of 4.26 M were used in combination with silver electrodes. [3] This study showed di-alkyl imidazolium cations could serve as co-catalysts for CO_2 reduction at unprecedentedly low onset potentials for selective reduction of CO_2 to CO, despite the presence of large amounts of water. Subsequent publications delved into possible mechanisms for HER suppression and enhancement of CO_2 reduction. [4-6] Leading possibilities for enhancement of CO_2 reduction include cation hydrogen-bond stabilization of transition states[14-16] and carbene-mediated coordination of CO_2 via cation complexes to activate CO_2. [14, 17-22] HER suppression mechanisms are typically centered around exclusion of water from interfaces. [7, 23]

Despite initial reports by Rosen and colleagues of pronounced enhancement of CO_2 reduction in aqueous electrolytes with very high ion concentrations, subsequent studies proceeded to focus on understanding how ion molecular structures influence CO_2 reduction in either neat ionic liquids or low concentration ionic liquid-supporting electrolyte blends. Dilute and neat ionic liquid electrolytes appear to be emphasized because dilute electrolytes maximize CO_2 transport due to low solution viscosity and neat ionic liquids maximize CO_2 solubility. For cases when ionic liquids are blended with solvent, acetonitrile has emerged as a common choice due to low viscosity, large electrochemical window, and high CO_2 solubility. [24]

Nonetheless, current mechanistic understandings of ionic liquid-mediated CO_2 electrochemical reduction focus more on molecular interactions between single ionic liquid ions and CO_2, while the influence of collective ion correlations and self-assembly on reactivity is often overlooked. Critically, current investigations appear to avoid intermediate concentrations, especially as ion concentrations begin to exceed dilute limits, which is around 1 M for an aqueous solution. For less polar solvents, such as acetonitrile, this crossover is shifted to lower concentrations. [25] Notably, this is the regime where ionic correlations are expected to emerge.

Therefore, we designed a systematic study of CO_2 reduction in ionic liquid solutions at varying concentrations, with a focus on intermediate concentrations, to illuminate the role of ionic correlations in electrochemical reactivity. Given that many electrochemical devices use electrolytes with ion concentrations that exceed the dilute limit, such insights will have broad implications that extend beyond CO_2 electrolysis processes.

Our core hypothesis is that ionic liquid-mediated CO_2 electrochemical reduction rates will exhibit non-monotonic scaling with electrolyte ion concentration and will be maximized at intermediate concentrations. Electrochemical reaction rates and pathways are closely related to the properties of electric double layers. Our hypothesis builds on recent findings from the surface force community showing that electric double layers often exhibit the most efficient screening, as evidenced by minimized electrostatic screening lengths, at intermediate concentrations, compared with dilute solution and high concentrations. [26-31] These observations stand in contrast to the classical Debye-Hückel theory, which predicts that increasing ion concentrations systematically increases the efficiency of electrostatic screening by decreasing screening lengths.

The non-monotonic relationship between ion concentrations and electrostatic screening lengths was interpreted as an indication that ionic correlations and clustering begin to emerge at high ion concentrations and that correlations cause many dissolved ions to become “bound” in effectively neutral aggregates. [26, 27,

[32] This formation of aggregates then reduces the population of "free" ions available to screen charged surfaces. As a result, electric double layers that form in highly concentrated electrolytes are much thicker, or less efficiently screened, than would be predicted via frameworks, like Debye-Hückel theory, which assumes ions are independently "free" to screen electrodes. [25-27, 30, 31, 33] Tuning ionic correlations by varying ion concentration should influence many properties of electrode-electrolyte interfaces that dictate electrocatalytic reactivity. [34-38]

We thus envision that the modulation of ionic correlations via concentration would allow us to achieve enhanced electrostatic screening, which would aid in breaking bonds and stabilizing transition states through localizing electric field gradients to electrode surfaces. Here, we describe our proof-of-concept study of how ion correlations and screening can be used as a complementary method for controlling electrochemical reactions. We chose the electroreduction of CO_2 to CO on silver electrodes in ionic liquid/acetonitrile blends with controlled water concentrations of 900-1100 ppm as our model reaction to illustrate how a holistic approach of considering double layer formation at electrocatalytic interfaces can qualitatively transform common reactivity metrics.

Our findings demonstrate that ionic strength can alter reactivity in ways that can rival the influence of the specific chemical structures of the ionic liquid ions studied. We used electrochemical kinetics approaches, including cyclic voltammetry (CV) measurements, to conduct ion concentration sweeps and reveal non-monotonic enhancement of CO_2 electroreduction rates for both co-catalytic and non-catalytic ionic liquid-based electrolytes (Fig. 1). We then performed chronoamperometry (CA) and product analysis studies (Fig. 2) to show that steady-state current densities and faradaic efficiencies reflect enhanced kinetics measured at intermediate concentrations. To gain insight into mechanisms of this rate enhancement, we performed *in-situ* electrochemical surface-enhanced Raman scattering (SERS) spectroscopy studies, which provide clues suggesting that rate acceleration originates in the enhancement of local potential gradients at concentrations that yield maximum current densities and faradaic efficiencies (Fig. 3).

Finally, we describe a noteworthy case where increases in ion concentration ultimately leads to cathode passivation through the formation of (bi)carbonate resulting from the reaction between CO_2 and OH^- (Fig. 4). This provides key insight into the role of the imidazolium ionic liquid in enhancing CO_2 reduction rates, suggesting new strategies for mitigating electrode passivation in organic electrolytes.

Results

Cyclic Voltammetry

We first analyzed the electrochemical behavior of ionic liquid solutions of varying concentrations separately under Ar- and CO_2-saturated solution conditions. Using 1-ethyl-3-methylimidazolium tetrafluoroborate (EMIm BF_4) in combination with a common supporting electrolyte salt tetrabutylammonium tetrafluoroborate (TBA BF_4) (Scheme 1), we examined ionic liquid-derived electrolytes with ions dissolved in acetonitrile at low concentrations that are commonly described in literature. We observed cyclic voltammetry (CV) results in agreement with prior studies for 25 mM EMIm BF_4 containing 0.1 M TBA BF_4, and neat EMIm BF_4 (Fig. 1A). [14, 19, 35, 39-41]

Presenting the same data but with mole fraction of EMIm BF_4 rather than concentration produces a very similar graph (Fig. S1) and does not change our observations and conclusions. We choose to present our findings as a function of ion concentration, which is an indication of the density of ions per unit volume. Ion density is a key metric describing the emergence of ion clustering and assembly, which occurs at ionic densities that bring neighboring ions to separation distances smaller than the Bjerrum length. [27] In contrast, mole fraction requires separately accounting size discrepancies between cations, anions, and solvents to determine when correlations emerge.

We then studied how the chemical structures of ions influence interfacial properties. Interestingly, the CV response of 125 mM EMIm BF_4 solution was comparable to that of 25 mM EMIm BF_4 + 0.1 M TBA BF_4 solution, exhibiting very similar onset potentials and current densities. Onset potentials are dictated by charge transfer activation energies, while current densities provide an indication of reaction rates.

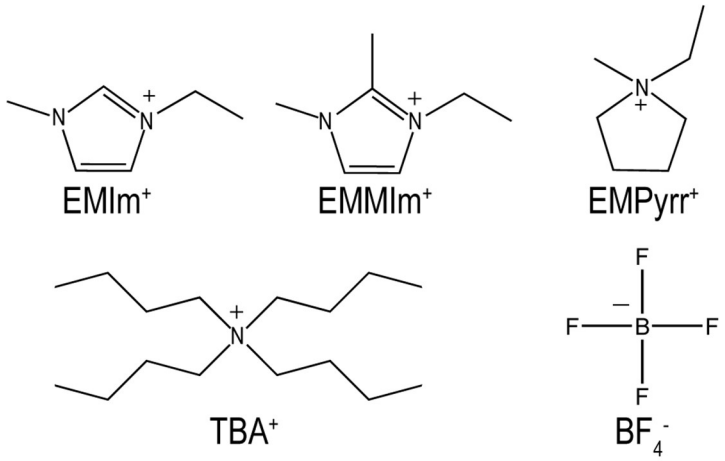

Scheme 1. Chemical structures of ionic liquid cations and anions used in this work.

Typically, EMIm BF_4 is thought to be a co-catalyst for the CO_2 electroreduction reaction, while TBA BF_4 is used as a supporting electrolyte to mitigate solution resistance losses. If the co-catalytic nature of EMIm

BF_4 is critical at these lower solution concentrations, then electrolytes with higher concentrations of EMIm BF_4 should yield higher current densities. The similarities in both onset potential and current density suggest that the total ion concentration has a larger influence on reactivity than the identity of the dissolved cations in the low concentration regime. Within the low concentration regime for these electrolytes, we conclude that CO_2 reduction is largely independent of specific ion properties but is instead proceeding via an outer-sphere mechanism, or direct electrode-CO_2 electron transfer.

Another notable finding from our work is that the onset potentials and current densities measured for neat EMIm BF_4 and the dilute (25 mM, no TBA BF_4) EMIm BF_4 solutions are similar. This surprising result, which is also observed for EMPyrr BF_4 and TBA BF_4 (Figs S4, S6), raises the possibility that reaction environments exhibited by some neat liquids may share analogies to reaction environments present in dilute electrolyte solutions, as ion clustering can dramatically suppress the availability of "free ions" to screen charged surfaces and localize potential gradients. Such an interpretation is consistent with discussions from the surface force community, where it is proposed that large electrostatic screening lengths present in ionic liquids cause them to behave analogously to dilute electrolytes, where very few "free" ions are available to redistribute and screen charged surfaces. [25, 26, 30, 33]

Most importantly, we observed a remarkable increase in CO_2 reduction rates, in the form of enhanced current densities, as we increased the concentration of EMIm BF_4 to exceed dilute limits (ca. 150 mM). At intermediate concentrations, such as 0.5 M EMIm BF_4 (Fig. 1A), we observed current densities that were almost double that of more dilute concentrations. Such high current densities were absent when electrolytes were purged with Ar (Fig. S2). Notably, onset potentials for CO_2 reduction did not vary greatly within this intermediate concentration regime. Hence, our concentration-dependent measurements indicate that the activation energy for CO_2 reduction reaction is similar across varied concentrations, but the reaction rate was substantially enhanced at intermediate concentration, as compared to the dilute and neat concentrations.

Small differences in onset potentials may be observed if an iR correction is used to account for solution resistance potential drops, where there is an associated potential drop required for current to flow in an electrochemical cell. In electrolytes with low conductivity, the potential experienced by reactants and products at the working electrode can be much smaller in magnitude than the potential applied by the potentiostat, and resulting voltammetry curves would appear linear rather than exponential with an increase in potential due to solution resistance. [42] As seen in Figure 1, the key intermediate concentration regimes that are the focus of our work exhibit CV curves that are more exponential in nature than linear, and accounting for iR drops would further increase the pronounced rate enhancement we observed.

Nevertheless, the 25 mM and neat EMIm BF_4 electrolytes do exhibit characteristics of solution resistance-limited rates (Fig. 1A), indicating that solution resistance plays a larger role at these two extreme concentrations. Solution resistance is dependent on cell geometry, so we maintained consistent distances and orientations between working and reference electrodes for all experiments. [42] To account for the solution resistance component of CV measurements, an iR correction can be applied, where solution resistance-related potential drop is calculated or measured and subtracted from the reported potential. When this data transformation is implemented, CV curves appear exponential. We present the untransformed data in the main text as we found that applying iR corrections will not change the trends and core features that we observe and present in this work.

In addition to solution conductivity, the identity of the proton donor involved in CO_2 reduction can have a large influence on reaction rates. In many cases, water is the only proton donor available to participate in CO_2 reduction, particularly when water is doped into aprotic solvents, like acetonitrile. In EMIm BF_4 solutions, imidazolium cations can also donate the acidic 2-site proton, which can cause EMIm cations to become the primary proton donor in intermediate-to-high concentration solution studied here. Future work evaluating how water concentration and the presence or absence of proton donors other than water influences reactivity would be illuminating in light of the universal enhancement of reaction rate with ion concentration we report here.

Overall, we conclude that changes in solution resistance and water activity are unlikely to be primary reasons for the rate enhancements we observe. By keeping the initial concentration of water constant among samples, we see variations in current density and faradaic efficiencies solely through changing cation structures (Fig. 1, Figs. S4, S6). If water activity or solution resistance were the dominant factor, we would expect to observe reactivity that was largely independent of cation structure. Notably, our results support recent works in the field, which increasingly suggest that cations play a leading role in determining CO_2 reduction activity[5, 43-45] and the likelihood that water activity or solution resistance could have higher order effects on observed reactivity would complement our key findings and conclusions.

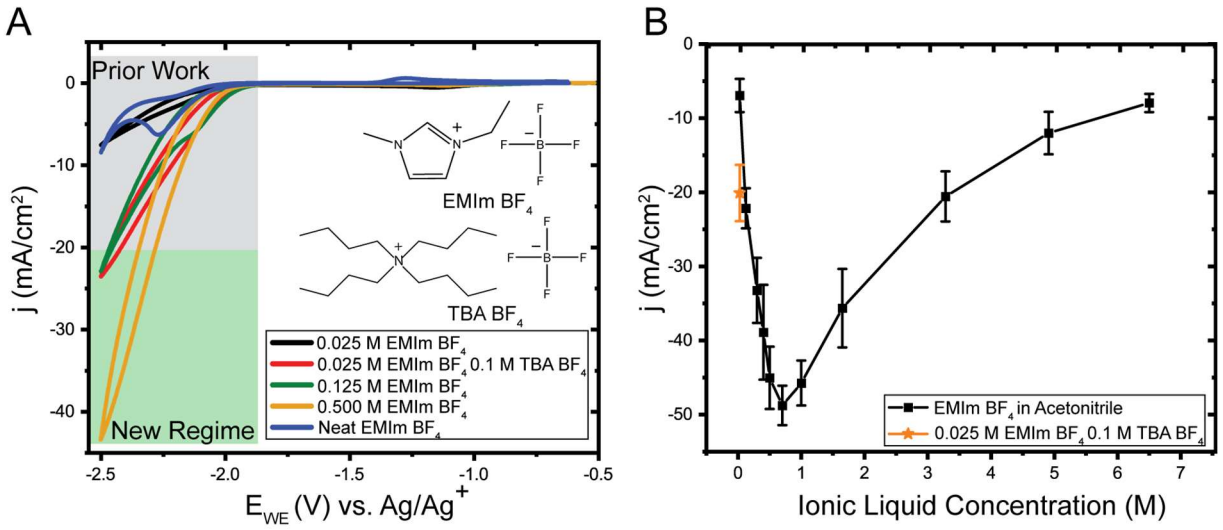

Figure 1. Non-monotonic concentration-dependent reactivity of CO_2 electrochemical reduction CO_2-saturated acetonitrile solutions of EMIm BF_4 at varying concentrations. (A) Representative CV results. Compared to the dilute and neat ionic liquid limits typically used in electrocatalysis studies, intermediate concentrations display a significant increase in current densities from CO_2 electrochemical reduction. (B) Non-monotonic concentration dependence of current densities. At -2.5 V vs. Ag/Ag^+, we observe pronounced increases in reactivity at intermediate concentrations of EMIm BF_4 in acetonitrile. Using the current densities at -2.5 V vs. Ag/Ag^+ as a representative value for a relatively high polarization, we find a remarkable average current density of 48.6 ± 3.0 mA/cm^2 at 0.7 M EMIm BF_4, which is more than double that of more traditional concentrations, such as neat EMIm BF_4 or 25 mM EMIm BF_4 + 0.1 M TBA BF_4. Each data point and error bar represent three independent trials, from which two representative CVs were used for each trial for a total of at least six values.

We also note that rigorous discussion of overpotentials for practical electrolysis of a complete electrochemical cell necessitates an understanding of both the cathodic and anodic reactions of interest. Conventionally, the cathodic reaction is depicted in Eq. 1, where CO_2, two protons, and two electrons react to form CO and H_2O. The corresponding anodic reaction, particularly in aqueous electrolytes, is the oxidation of water into two protons and one oxygen atom (Eq. 2).

$$H_2O \rightarrow 2H^+ + \tfrac{1}{2}O_2 + 2e^- \quad (2)$$

Using these two half-reactions, the overall thermodynamic potential is -1.33 V. [3, 46] As written, water should be neither generated nor consumed between the two half-reactions. During our trials, we observed a consistent increase in water content in the anolyte after CA, suggesting the circuit was completed by anodic

reactions other than water oxidation. [16, 47] Prior works indicate that -1.5 V vs. Ag/Ag^+ is the onset potential for the cathodic reaction shown in Eq. (1) in acetonitrile solutions of ionic liquids, [47] and we find this value to be the appropriate potential to use for calculating overpotentials. Taken together, we conclude that the onset potentials we report in this work are comparable to prior studies.

We then conducted a study on a wide concentration range of EMIm BF_4 with a particular focus on the intermediate concentrations. We observed a non-monotonic enhancement of reaction rate with concentration, with a maximum average current density at 0.7 M EMIm BF_4 (Fig. 1B). CV is used primarily to study electrochemical reaction kinetics, so our results suggest that the maximum reaction rate enhancement of CO_2 reduction occurs at 0.7 M EMIm BF_4. Beyond this concentration, however, the reactivity decreased such that current densities of the neat ionic liquid became similar to that of the 25 mM electrolyte.

Chronoamperometry

Figure 2 shows results from 3-hour-long electrolysis experiments under well-mixed conditions. Generally, the trends observed in CA experiments align well with the CV results. The steady-state current densities and corresponding faradaic efficiencies for CO reached a maximum at 0.9 M EMIm BF_4 rather than the 0.7 M suggested by CV. In addition to CA experiments, we used nuclear magnetic resonance (NMR) to compare changes in electrolyte composition before and after experiments. For EMIm BF_4, we observed formation of a carboxylate adduct in catholytes that has previously been reported in literature. [19, 48, 49] The abundance of this adduct was positively correlated with the current density of corresponding electrolytes and was the most pronounced in electrolytes with intermediate concentrations (Fig. S3 and Table S1).

Reduction of CO_2 with water as the proton donor is known to generate HCO_3^- through reaction between CO_2 and OH^- anions and is a major contributor to low faradaic efficiencies for CO_2 reduction reactions in alkaline or near-neutral pH media. [43, 50-52] Meanwhile, prior studies suggested that the carboxylate adduct spontaneously forms when EMIm cations and HCO_3^- coexist in acetonitrile. [47] We conclude that the formation of adduct at the C2 position of the imidazolium cation ring in our study is more likely a byproduct of the reduction of CO_2 through the full reaction:

$$3CO_2 + 2EMIm^+\text{-}H + 2e^- \rightarrow CO + 2EMIm^+\text{-}COO^- + H_2O \quad (3)$$

Indeed, the water content in catholytes increased by 1000 to 2000 ppm after 3-hour electrolysis, matching the trend predicted by the equation and suggesting that imidazolium cations serve as a primary proton donor for CO_2 reduction in EMIm BF_4 electrolytes.

We observed a similar non-monotonic trend in steady-state current densities and faradaic efficiencies for 1-ethyl-1-methylpyrrolidinium tetrafluoroborate (EMPyrr BF_4), an ionic liquid that is not considered a co-catalyst for CO_2 electroreduction and cannot act as a proton donor (Fig. 2). In CA studies for EMPyrr BF_4, we found that the steady-state current densities and faradaic efficiencies reach a maximum at 0.5 M EMPyrr BF_4, instead of the maximum at 0.9 M observed for EMIm BF_4. Using CV, we measured the largest current densities for the 125 mM EMPyrr BF_4 solution (Fig. S4), which may be due to both electrochemical cell setup, as well as electrode cycling history. For practical considerations, CA results are more directly applicable to electrolysis applications. NMR results indicated no significant change in the composition of the electrolyte after the electrolysis experiments (Fig. S5).

In both EMIm BF_4 and EMPyrr BF_4, acetonitrile decomposition accounts for the reduced faradaic efficiency at low concentrations, [53] since H_2 production was absent and ^{1}MR showed similar impurity peaks for catholytes with different contents (Figs. S3, S5). At high concentrations, drops in steady-state current densities and faradaic efficiencies likely arise from ionic liquid decomposition[41, 49] since significant H_2 production was not observed, nor was the formation of carbonate species. Yet, due to the low current densities corresponding to these concentrations, ionic liquid decomposition products are not abundant enough to be detected by NMR of bulk electrolyte.

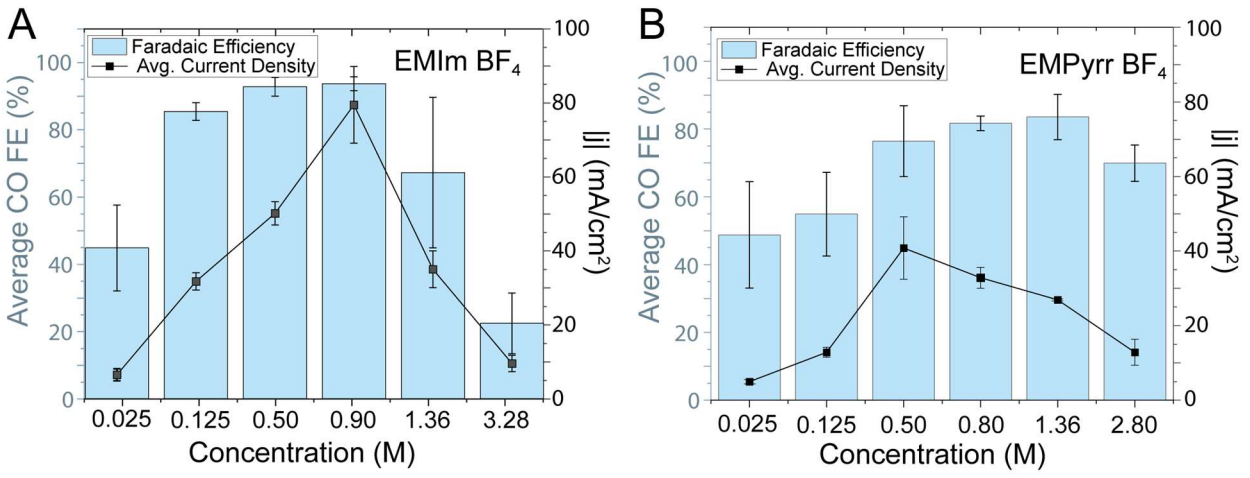

Figure 2. Steady-state faradaic efficiencies (FE) for CO production and current densities (j) obtained over the course of hours 1-3 of chronoamperometry at -2.5 V vs. Ag/Ag^+ on Ag electrodes for varying concentrations of (A) EMIm BF_4, and (B) EMPyrr BF_4 in acetonitrile solvent. While EMIm BF_4 displayed

higher steady-state current densities and faradaic efficiencies at intermediate concentrations, EMIm BF_4 and EMPyrr BF_4 share a similar non-monotonic enhancement of both current densities and faradaic efficiencies along with concentrations, suggesting that this enhancement is not ion-specific. Each data point represents an average and standard deviation obtained from seven time points collected for each sample.

We then tested the supporting electrolyte to further evaluate its role in the reduction reaction. CV trials with TBA BF_4 exhibited very similar reactivity trends (Fig. S6) as EMIm BF_4 and EMPyrr BF_4, where the peak current density is achieved at concentrations lower than 1 M. Prior works concluded that tetraalkylammonium-based salts are not co-catalysts for CO_2 electroreduction and mediate the reaction via an outer-sphere mechanism, [24, 54] which may explain the lower current densities for TBA BF_4 when compared with EMIm BF_4.

Surface-enhanced Raman spectroscopy (SERS)

With our observation of a concentration-dependent reactivity for TBA BF_4, we posit that the role of TBA BF_4 both reduces solution resistance and impacts CO_2 electroreduction by influencing interfacial properties. The higher current densities and faradaic efficiencies we observed for EMIm BF_4 still strongly point to imidazolium-based ionic liquids functioning as a co-catalyst, where the non-monotonic behavior is amplified by the co-catalytic nature of EMIm cations. The non-monotonic trend that we observe for both co-catalytic and non-catalytic ionic liquids provides evidence suggesting that this behavior is generalizable to different ion structures. We propose that difference in electric potential gradients mediated by the collective assembly of ions is a likely mechanism influencing reactivity. Thus, we used *in situ* SERS to gain molecular level insights into the potential-modulated assembly of ions in the electric double layer and determine how electric potential gradients depend on the concentration of ionic liquid ions (Fig. 3).

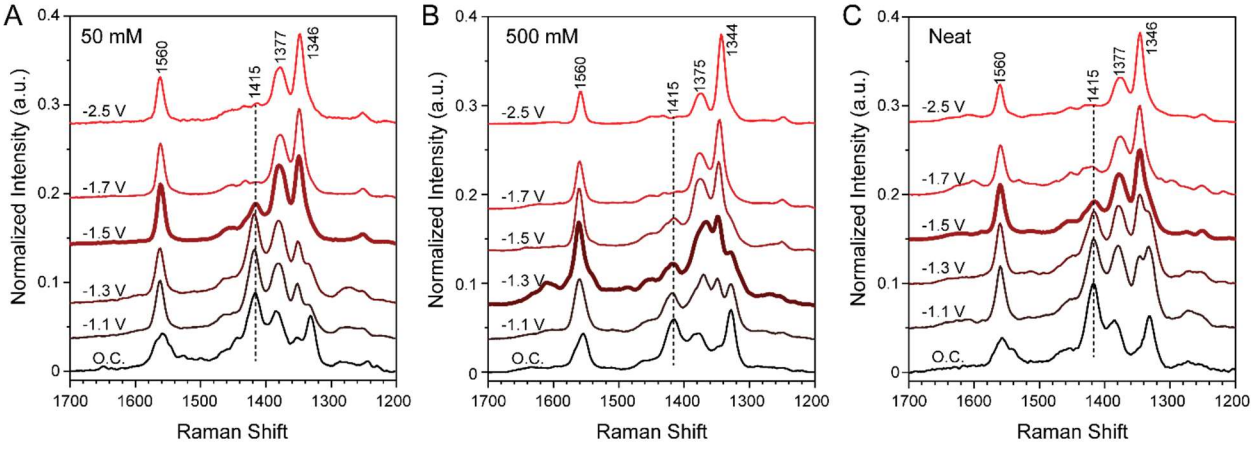

Figure 3. *In situ* SERS spectra of (A) 50 mM EMIm BF_4, (B) 500 mM EMIm BF_4, and (C) neat EMIm BF_4 in the ring deformation region in forward potential sweeps. Intensities of peaks at 1560, 1375, and 1344 cm^{-1} gradually increase, and the peak at 1415 cm^{-1} gradually decreases when the potential is decreased from open-circuit potential to -2.5 V vs. Ag/Ag^+ in all three cases (Fig. S7). Nonetheless, the 500 mM EMIm BF_4 exhibits more rapid changes in relative peak intensities compared with 50 mM and neat EMIm BF_4. While the intensity ratio of the 1344 cm^{-1} peak over the 1415 cm^{-1} peak is initially smaller than 1, it is inverted before the applied potential reaches -1.3 V for 500 mM EMIm BF_4. In contrast, at least -1.5 V was required to observe a similar inversion in the peak ratio for 50 mM and neat EMIm BF_4 (Fig. S10). At each concentration, the SERS spectrum from the potential required to invert the peak ratio between 1344 and 1415 cm^{-1} is bolded for a clearer comparison. O.C. stands for open-circuit potential. *In situ* SERS spectra with full wavenumber range and intermediate potential steps are shown in Figure S8.

For EMIm BF_4 solutions, the intensity of SERS peaks at 1560, 1376, and 1344 cm^{-1} in the imidazolium ring fingerprint region increase during cathodic potential sweeps, [55, 56] which is accompanied by a decrease in the intensity of a peak at 1415 cm^{-1}. Identical spectral changes occurred in both CO_2-saturated (Fig. 3) and Ar-purged solutions (Fig. S9), which can be interpreted as reorientation of $EMIm^+$ in response to the electric fields. [57, 58] We use the intensity ratio of the peak at 1344 cm^{-1} to the peak at 1415 cm^{-1} as an indicator of the extent of $EMIm^+$ reorientation. This ratio shows a more rapid increase with the applied potential and reaches a higher value at -2.5 V for 500 mM EMIm BF_4 compared with 50 mM and neat EMIm BF_4 (Fig. 3, Figs. S8, S10). This indicates a more pronounced reorientation of EMIm cations in 500 mM solution as a function of applied potential, indicating stronger local electric fields exist in solutions with intermediate ionic concentrations.

We also studied the concentration-dependent behavior of 1-ethyl-2,3-dimethylimidazolium tetrafluoroborate (EMMIm BF_4), an ionic liquid that was reported to display higher reactivity than EMIm BF_4 at low concentrations due to the methylation of the C2 site that prevents carbene formation. [14, 19, 41] We found that solution ion concentration critically determines if methylation enhances or detracts from reactivity. We successfully reproduced the high activity of CO_2 reduction using EMMIm BF_4 at a low concentration (25 mM) with 0.1 M TBA BF_4 supporting electrolyte. However, increasing the concentration of EMMIm BF_4 to 125 mM and higher resulted in significantly lower current densities and faradaic efficiencies in 3-hour electrolysis (Fig. 4A).

Upon further examination, we found that the CVs associated with higher concentrations of EMMIm BF_4 yielded vastly different shapes between the initial and subsequent cycles (Figs. S12-S15), unlike EMIm BF_4 which maintained the same shape between cycles (Fig. S11). Although the initial cycles for EMMIm

BF typically yielded current densities greater than -20 mA/cm^2 and displayed the same non-monotonic enhancement as EMIm BF_4 (Fig. S16), the following cycles appeared to allow little or no CO_2 electroreduction. Steady-state current densities also showed quick drops in current density upon initial polarization, and faradaic efficiencies reached a maximum at 125 mM EMMIm BF_4 (Fig. 4).

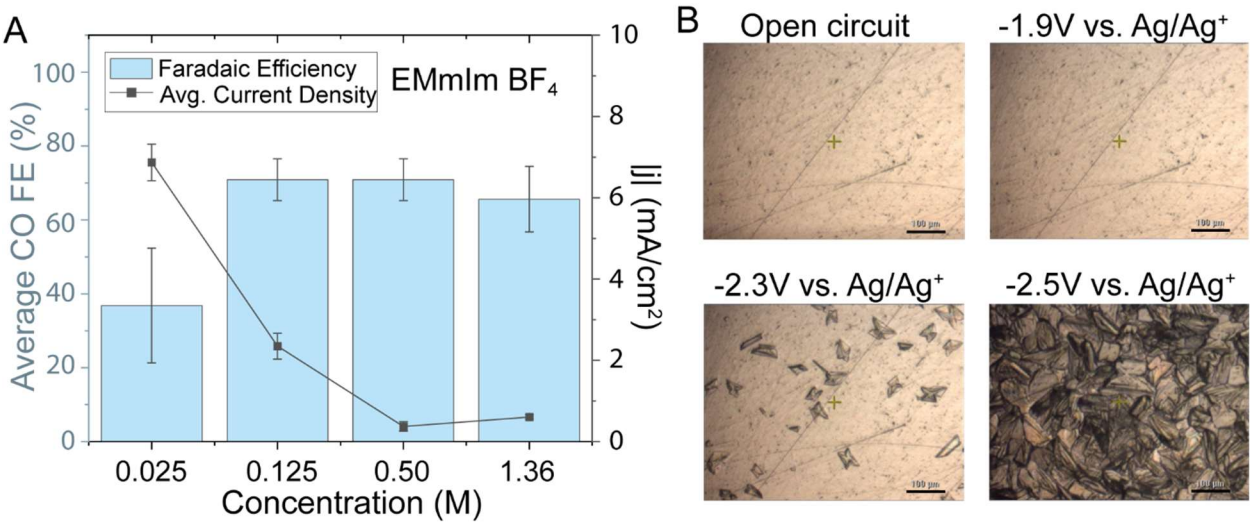

Figure 4. CA and FE results for CO_2-saturated acetonitrile solutions of EMMIm BF_4 at different concentrations and representative images of electrode passivation via the formation of EMMIm HCO_3. (A) CA and FE results. EMMIm BF_4 is considered a better co-catalyst than EMIm BF_4 in previous literature at dilute concentrations. However, EMMIm BF_4 displays an unexpected decrease in steady-state current densities at concentrations beyond 125 mM, while faradaic efficiencies at these concentrations are near constant. (B) Nucleation and growth of EMMIm HCO_3 crystals in a CO_2-saturated acetonitrile solution of 0.125 M EMMIm BF_4 at 10x magnification. Crystals started to form at potentials exceeding -2.3 V. These crystals likely limit mass transport of reactants and products across interfaces, accounting for the decrease in reactivity at relatively higher concentrations shown in (A). Interestingly, onset potentials for crystallization, crystal morphology, and crystal growth rate vary drastically with solution conditions (Figs. S18-S21). Scale bars in (B) stand for 100 μm.

To understand this surprising drop in reactivity, we used *in situ* SERS and optical microscopy to observe electrode surfaces as reactions proceeded. When electrolyte solutions were saturated with CO_2, we observed the potential-dependent nucleation and growth of crystals even when the concentration of EMMIm BF_4 was as low as 50 mM (Figs. 4B, S18, and S19). Interestingly, similar crystals formed in CO_2-saturated solutions of EMMIm Br and EMMIm TSFI at potentials close to the onset potential for CO_2 reduction (Figs. S20, S21), suggesting that the crystallization was independent of anion identity and was derived from processes

related to CO_2 reduction. Indeed, NMR analysis indicates that the crystals are EMMIm HCO_3, which is insoluble in acetonitrile (Figs. S22, S23). Therefore, we deduce that initial CO_2 reduction in EMMIm BF_4 electrolytes quickly built up HCO_3^- at electrode-electrolyte interface, which then precipitates with EMMIm cations to rapidly passivated electrode surfaces.

Electrode passivation, along with carbonate or bicarbonate formation, are major hurdles that must be overcome to achieve efficient CO_2 electroreduction. The onset potential and rate of crystal nucleation and growth varied with the corresponding anion or when we added supporting electrolytes such as TBA BF_4. These changes in rate of electrode passivation suggest promising pathways towards combatting the issue of electrode passivation by disrupting crystal formation via tuning interfacial assembly. Further, these results offer an explanation for the high activity of EMIm BF_4 – it is able to form a carboxylate with HCO_3^- in solution, decreasing the bicarbonate concentration near the electrode surface. In doing so, EMIm BF_4 appears to mitigate the problem of bicarbonate formation to an extent, a pathway that was unavailable to the other ionic liquids we examined.

Discussion

The general nature of non-monotonic concentration-dependent reactivity in different ionic liquid-derived electrolytes, together with *in situ* SERS results on EMIm BF_4, indicate that differences in CO_2 reduction rates originate from changes in screening efficiency as a non-monotonic function of ion concentration (Fig. 5). To substantiate the plausibility of this mechanism, we performed a mean-field scaling theory analysis of how the Debye screening length for ionic liquid-acetonitrile blends depends on solution concentration. A more detailed discussion of the limitations and implications of the Debye-Hückel theory and our scaling analysis can be found in the Supporting Information.

Briefly, dilute electrolyte theory, such as Debye-Hückel theory, predicts that electrostatic screening lengths, and correspondingly, double layer thicknesses, arise from competition between ion entropy of mixing, which favors thicker double layers, and ion-surface Coulomb interactions that favor thinner double layers. In the dilute limit, the key length scale associated with screening is the Debye screening length, which can be calculated from knowledge of ion concentration, ion valence, and solution permittivity. Using the Debye length as a proxy for the electric double layer thickness, dilute theory predicts that electrostatic screening lengths and double layer thicknesses always decrease, indicating enhanced screening, as ion concentration increases.

Yet, dilute electrolyte theories neglect ion-ion interactions, leading to predicted Debye lengths that become smaller than any plausible dimension of individual ions as concentration is increased **(Fig S24)**. In this

limit, ion-ion interactions drive ion clustering into charge-neutral aggregates as the ion concentration is further increased. Cluster formation decreases the concentration of "free ions" available to participate in screening, leading to a disparity between the "free ion" concentration and total number of ions per unit volume. Indeed, recent work on ionic liquid-solvent blends and aqueous electrolytes from the surface forces community indicates that a primary signature of ion-ion correlations is deviation of measured electrostatic screening lengths from calculated Debye length, which arises at around 1 M. [25, 27]

Taken together, we propose that ionic liquid electrolytes with either dilute or high concentrations can have relatively long screening lengths at the order of several nanometers due to a scarcity of ions and the clustering of ions to neutral aggregates, respectively, leading to inefficient screening. [28-30] At intermediate concentrations, the transition between dilute and correlated regimes should yield double layers with much shorter screening lengths, as there are sufficient ions to efficiently screen surface potentials without the presence of excessive impeding ion clusters.

More broadly, thin double layers yield steeper potential gradients as applied potentials are screened within short distances, and the magnitude of the local potential gradient is key in determining electrochemical reaction rates. [43, 59, 60] In strongly-screening cases, large potential gradients will enhance reactivity by creating polarized environments that require less energy for bonds to bend or break. Similar themes of electric field gradients enhancing reactivity are found in biology, where potential gradients in enzyme active sites orient and break chemical bonds or stabilize important reaction intermediates. [59-62]

In CO_2 electroreduction, a key intermediate is $CO_2^{\bullet-}$, an unstable and bent negative radical with a permanent dipole. Therefore, a compact and strongly-screening double layer achieved at intermediate concentrations would more effectively stabilize $CO_2^{\bullet-}$, leading to the maximum rate of CO_2 electroreduction. In contrast, electrolytes in dilute and correlated regimes, where ionic screening lengths are longer, would be expected to form an environment that is less amenable to stabilizing charged or polar intermediates and lead to lower reactivity.

Overall, our scaling theory analysis links the regime of highest expected reactivity with that of the most efficient double layer screening and suggests that intermediate ion concentration may be a generally advantageous electrolyte regime for electrocatalytic processes. Yet, we caution that the electric double layer is a dynamic and complex environment during electrochemical reactions that cannot be comprehensively described using classical electrolyte theory, especially at high ionic liquid concentrations where ionic liquid assembly plays a major role. [63] Future refinement of this proposed mechanism would require new ways of

measuring electrolyte structure and potential distributions at interfaces, molecular dynamics simulations, or other approaches that yield further molecular detail on the role of ionic correlations.

Our interpretation explains the concentration-dependent reactivity trend we observe, where reaction rates are non-monotonic with ion concentration. Specifically, intermediate concentrations create local reaction environments that better facilitate the formation of intermediates and turnover to products. Importantly, this characteristic of compact and thin double layers is not restricted to only co-catalytic ionic liquids, as evidenced by the EMPyrr BF_4 studies. We anticipate that our findings have applications extending far beyond CO_2 electroreduction and may prove useful in both understanding, as well as controlling energy-intensive electrochemical reactions such as nitrogen fixation.

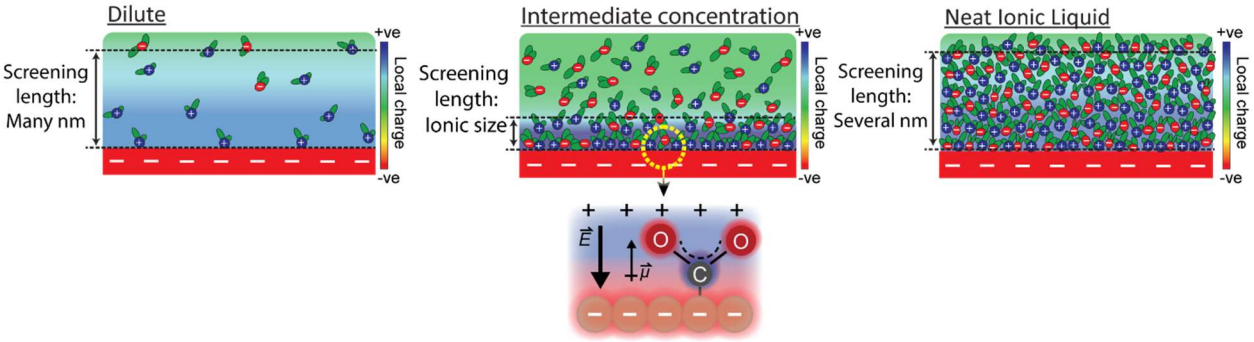

Figure 5. We propose that by changing concentration as a proxy for changing ionic correlations, we can drastically enhance CO_2 electroreduction rates by modulating the double layer thicknesses and electrostatic screening lengths. For dilute and concentrated regimes, a lack of ions and excessive ionic correlations, respectively, induce the formation of thick double layers. At the crossover between the dilute and correlated regimes, intermediate concentrations facilitate formation of thin double layers, which can screen electrode potentials across molecular level distances and sustain large gradients in electric field strength. At these intermediate concentrations, the screening length approaches ionic sizes, forming a double layer that is more efficient at electrostatic screening and creating a large potential gradient. This large potential gradient near electrode surfaces would stabilize intermediates and transition states.

Conclusions and Future Work

In this work, we show that ionic liquid-based electrolytes exhibit pronounced non-monotonic reactivity-concentration scaling for electrochemical CO_2 reduction to CO. Our conclusions are supported by cyclic voltammetry studies of reaction kinetics as well as steady-state electrolysis experiments. Notably, our findings are general for multiple classes of ionic liquids and should also extend to other solvents.

To substantiate our conclusions, we performed SERS and found that more strongly screening environments were formed near electrode surfaces at intermediate concentrations, where we observed higher reactivity. This is evidenced by more pronounced changes to potential-dependent ring deformation at intermediate concentrations, observed as shifts in the Raman scattering exhibited by imidazolium ring structure.

We interpret our data set to indicate that electrostatic screening is more efficient at intermediate concentrations, leading to thinner electric double layers, which facilitate CO_2 reduction via near-surface localization of potential gradients. While EMMIm BF_4 does exhibit a nonmonotonic concentration-reactivity trend based on CV data, chronoamperometry measurements are hindered by precipitation of an insulating crystalline layer over time, which inhibits further CO_2 electrochemical reduction. We determined that this crystalline precipitate occurs due to formation of HCO_3^- species, which drive the nucleation and growth of a crystalline insulating EMMIm HCO_3^- film under reaction conditions. This important result suggests that the EMIm BF_4 reactivity is partially owed to the ability of the C2 position to coordinate HCO_3^- and also offers potential strategies to combat electrode passivation.

In summary, our findings have important implications for understanding how tuning electric double layer assembly, and in turn, local reaction environments, could enhance or enable better control over reactivity in important electrochemical reactions. We show that tuning EDL screening efficiency can significantly influence the electrocatalytic reaction both in terms of current density and faradaic efficiency. Our preliminary scaling analysis suggests that the Debye screening length can be a simple and useful metric for analyzing screening efficiency by showing that the range of concentrations in which the Debye screening length approaches ion sizes is an ideal regime to explore for enhanced reactivity. Notably, our proposed theory is not ion or solvent specific, and can be generalized to electrochemical processes requiring different electrolyte compositions or more energy-intensive electrocatalytic reactions. Our findings show that the liquid side of electrode-electrolyte interfaces can be used to sculpt reaction landscapes in ways that can rival the influence of the solid side of electrochemical interfaces.

Experimental Details

Chemicals. The ionic liquids used in the preparation of the electrolytes were: 1-ethyl-3-methylimidazolium tetrafluoroborate (EMIm BF_4, >98% purity, Iolitec), 1-ethyl-2,3-dimethylimidazolium tetrafluoroborate (EMMIm BF_4, 97% purity, Alfa Aesar), 1-ethyl-1-methylpyrrolidinium tetrafluoroborate (EMPyrr BF_4, >98% purity, Iolitec), and tetrabutylammonium tetrafluoroborate (TBA BF_4, 99% purity, Sigma Aldrich). All ionic liquids were used without further purification. Nuclear magnetic resonance (NMR) and electrochemical analysis were used to confirm purity upon receiving the chemicals. Ultrapure water (Milli-Q, ≥18.2 MΩcm) was used in all experiments. HPLC grade Acetonitrile and ethanol were purchased from

Fisher Chemicals and Decon Labs. Inc, respectively. Deuterated dimethylsulfoxide (DMSO-d6) was from Sigma-Aldrich. CO_2 and Ar gas were purchased from Airgas. In the synthesis of Ag nanoparticles, silver nitrate was from Alfa Aesar, sodium borohydride was from Sigma-Aldrich, and sodium citrate dihydrate was from Fisher Bioreagents.

Electrochemical Methods. Electrochemical measurements were performed in borosilicate glass cells and were carried out using a BioLogic VSP potentiostat. Electrolyte solutions were comprised of ionic liquids dissolved in acetonitrile. Due to the hygroscopic nature of acetonitrile, water content of stock acetonitrile ranged from <100 ppm to 500 ppm. Water is a potential source of protons for CO_2 electroreduction, so water content is known to impact observed reactivity. To control the influence of trace water, water was systematically added to the acetonitrile to reach concentrations of 900-1100 ppm to maintain consistent electrolyte conditions between trials. In parallel experiments, we undertook extensive efforts to dry all electrolyte materials and fond that CO_2 reduction is suppressed in extensively dried ionic liquid-based electrolytes, consistent with literature reports. [4, 64, 65] Hence, water is an essential proton source during ionic liquid-mediated CO_2 reduction, and our results substantiate this conclusion, as elaborated in the Results and Discussion.

Measurements of water content were carried out using a Mettler Toledo C10S Coulometric Karl Fischer Titrator. For cyclic voltametric (CV) and chronoamperometric (CA) measurements, the working electrode was a polycrystalline Ag electrode (BASi) with a geometric surface area of 0.071 cm^2. All current densities presented in this work are normalized to geometric surface area. The working electrodes were polished to a mirror finish based on established protocols using 15 μm, 3 μm, and 1 μm diamond polish and then 0.05 μm alumina (BASi) to a mirror finish prior to sonication to remove adsorbed alumina. Quantitative agreement with prior studies was achieved using this method. For all electrochemical measurements, we used an Ag/Ag^+ non-aqueous reference electrode and a coiled platinum wire as a counter electrode. A ferrocene/ferrocenium redox couple was used initially to confirm the applicability of a Ag/Ag^+ (0.01 M $AgNO_3$) non-aqueous reference previously described for acetonitrile-containing electrolytes. Since the silver surface readily oxidizes in the potential range near the ferrocene/ferrocenium redox couple, all potentials used in this work are referenced to the Ag/Ag^+ (0.01 M $AgNO_3$) reference. [46] Electrolyte solutions were purged for 20 minutes prior to electrochemical measurements using either Ar or CO_2 gas.

For CV measurements, we designed and 3D-printed caps using chlorinated polyethylene elastomer filament (Prusa) for the one-compartment batch electrochemical cell to ensure reproducible cell geometry to control for effects of solution resistance across trials. All CV measurements were carried out at scan rates of 100 mV/s.

Product Analysis. We studied the products of electrolysis and determined corresponding faradaic efficiencies using a custom-made gas-tight 2-compartment cell in CA studies. The compartments were separated using a Nafion 117 membrane and were continuously stirred as well as purged with CO_2. The compartments were well-mixed to eliminate transport effects (Figure S25). Potentials of -2.5 V were held for 3 hours, where steady state was reached after 1 hour.

Nafion 117 membranes for chronoamperometric studies were prepared according to literature prior to use. [19, 66, 67] In brief, as-received membranes precut to desired dimensions were immersed in 3 wt% H_2O_2 aqueous solution, Milli-Q Ultrapure water, 1 M H_2SO_4 aqueous solution, and Milli-Q Ultrapure water again in sequence. All solutions were heated to 80 °C, and each step took 1 hour. After preparation, we stored membranes in 0.1 M TBA BF_4-acetonitrile solution when not in use, and the membranes were rinsed with Milli-Q Ultrapure water and acetonitrile every time prior to use.

Gaseous products of CA experiments were analyzed every 20 minutes using a gas chromatograph (SRI Multiple Gas Analyzer #5) equipped with a thermal conductivity detector (TCD) and a flame-ionization detector (FID) equipped with a methanizer. A HayeSep D column was connected to the TCD while the FID was connected to a HayeSep D and a Molesieve 5A column (Restek). Ultrahigh purity grade He (Airgas) was used as the carrier gas.

The faradaic efficiency was calculated by: [68]

$$FE(\%) = \frac{\frac{v}{60s/min} \times \frac{y}{24{,}000cm^3/mol} \times N \times F}{i} \times 100\%$$

where v = 9.2 sccm is the flow rate of CO_2, y is the concentration of product measured from GC in the unit of mole fraction, N = 2 is the number of electrons consumed to convert one CO_2 molecule to one CO, F = 96500 C mol^{-1} is the Faraday constant, and i is the total current passing through the working electrode in the unit of A.

We performed NMR spectroscopy using a 400 MHz NMR spectrometer (Bruker Avance) with a BBFO probe to evaluate the electrolyte composition before and after CA experiments through 1H NMR and 13C NMR. DMSO-d6 was used as the solvent.

SERS Measurements. Electrochemical surface-enhanced Raman scattering (SERS) measurements were carried out using a single-compartment PTFE electrochemical cell with a polished L-shaped Ag working electrode (Shanghai Fanyue Electronic Technology Co. Ltd) prepared by drop-casting Ag nanoparticles onto the surface to achieve enhancement. Ag nanoparticles were synthesized based on a previously reported

method. [69] The counter electrode was a polished and coiled Pt wire, while the reference electrode was a non-aqueous Ag/Ag^+ (0.01 M $AgNO_3$) reference. The electrolyte was purged with either Ar or CO_2 for 20 minutes prior to conducting the measurements. SERS spectra were collected using a Thermo-Fisher Scientific DXRxi Raman Imaging Microscope with a 532 nm excitation laser and at 10x magnification. The laser power was 9.0 mW, and the acquisition time was 0.033 s (30 Hz) with 300 scans for all measurements. Potential-dependent SERS spectra were collected by sweeping the potential from -0.7 V to -2.5 V and then back to -0.7 V. Optical images of the working electrode surface were also captured using the same Raman imaging microscope in video mode.

AUTHOR INFORMATION

Corresponding Author

* Matthew A. Gebbie – Department of Chemical and Biological Engineering, University of Wisconsin – Madison, Madison, Wisconsin 53706, United States; https://orcid.org/0000-0002-4619-4002; Email: gebbie@wisc.edu

Author Contributions

The manuscript was written through contributions of all authors. All authors have given approval to the final version of the manuscript.

Supporting Information. Further discussion of scaling theory and additional experimental data.

Funding Sources

The authors acknowledge support from the Department of Chemical and Biological Engineering at the University of Wisconsin-Madison and the Wisconsin Alumni Research Fund. M. A. G. acknowledges support from the Michael F. and Virginia H. Conway Assistant Professorship. B. L. acknowledges support from the Fenton-May Graduate Fellowship.

Notes

The authors declare no competing financial interest.

ACKNOWLEDGMENT

This work used facilities and instrumentation at the UW-Madison Wisconsin Centers for Nanoscale Technology (wcnt.wisc.edu) partially supported by the NSF through the University of Wisconsin Materials Research Science and Engineering Center (DMR-1720415). The Bruker AVANCE 400 NMR spectrometer was supported by NSF grant CHE-1048642.

TOC Image:

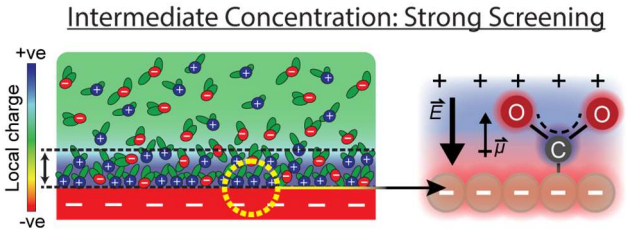

REFERENCES

1. Chandrasekaran, K.; Bockris, J. O. M. In-situ spectroscopic investigation of adsorbed intermediate radicals in electrochemical reactions - CO_2^-. *Surface Science* **1987**, *185*, 495-514.

2. Hori, Y.; Wakebe, H.; Tsukamoto, T.; Koga, O. Electrocatalytic process of CO selectivity in electrochemical reduction of CO_2 at metal electrodes in aqueous media. *Electrochimica Acta* **1993**, *94*, 1833-1839.

3. Rosen, B. A.; Salehi-Khojin, A.; Thorson, M. R.; Zhu, W.; Whipple, D. T.; Kenis, P. J. A.; Masel, R. I. Ionic Liquid–Mediated Selective Conversion of CO_2 to CO at Low Overpotentials. *Science* **2011**, *334*.

4. Rosen, B. A.; Zhu, W.; Kaul, G.; Salehi-Khojin, A.; Masel, R. I. Water Enhancement of CO_2 Conversion on Silver in 1-Ethyl-3-Methylimidazolium Tetrafluoroborate. *Journal of The Electrochemical Society* **2012**, *160* (2), H138-H141.

5. Bondue, C. J.; Graf, M.; Goyal, A.; Koper, M. T. M. Suppression of Hydrogen Evolution in Acidic Electrolytes by Electrochemical CO_2 Reduction. *Journal of the American Chemical Society* **2021**, *143* (1), 279-285.

6. Rosen, B. A.; Haan, J. L.; Mukherjee, P.; Braunschweig, B.; Zhu, W.; Salehi-Khojin, A.; Dlott, D. D.; Masel, R. I. In Situ Spectroscopic Examination of a Low Overpotential Pathway for Carbon Dioxide Conversion to Carbon Monoxide. *The Journal of Physical Chemistry C* **2012**, *116* (29), 15307-15312.

7. Wang, Y.; Hayashi, T.; He, D.; Li, Y.; Jin, F.; Nakamura, R. A reduced imidazolium cation layer serves as the active site for electrochemical carbon dioxide reduction. *Applied Catalysis B: Environmental* **2020**, *264*.

8. Faggion, D., Jr.; Goncalves, W. D. G.; Dupont, J. CO_2 Electroreduction in Ionic Liquids. *Front Chem* **2019**, *7*, 102.

9. Appel, A. M.; Bercaw, J. E.; Bocarsly, A. B.; Dobbek, H.; DuBois, D. L.; Dupuis, M.; Ferry, J. G.; Fujita, E.; Hille, R.; Kenis, P. J.; et al. Frontiers, opportunities, and challenges in biochemical and chemical catalysis of CO_2 fixation. *Chemical Reviews* **2013**, *113* (8), 6621-6658.

10. Alvarez-Guerra, M.; Albo, J.; Alvarez-Guerra, E.; Irabien, A. Ionic liquids in the electrochemical valorisation of CO_2. *Energy & Environmental Science* **2015**, *8* (9), 2574-2599.

11. Welton, T. Ionic liquids: a brief history. *Biophysical Reviews* **2018**, *10* (3), 691-706.

12. Rogers, R. D.; Seddon, K. R. Ionic Liquids— Solvents of the Future? *Science* **2003**, *302*, 792-793.

13. Sheldon, R. Catalytic reactions in ionic liquids. *Chemical Communications* **2001**, (23), 2399-2407.

14. Lau, G. P. S.; Schreier, M.; Vasilyev, D.; Scopelliti, R.; Gratzel, M.; Dyson, P. J. New Insights Into the Role of Imidazolium-Based Promoters for the Electroreduction of CO_2 on a Silver Electrode. *Journal of the American Chemical Society* **2016**, *138* (25), 7820-7823.

15. Ratschmeier, B.; Braunschweig, B. Cations of Ionic Liquid Electrolytes Can Act as a Promoter for CO_2 Electrocatalysis through Reactive Intermediates and Electrostatic Stabilization. *The Journal of Physical Chemistry C* **2021**, *125* (30), 16498-16507.

16. Wang, Y.; Hatakeyama, M.; Ogata, K.; Wakabayashi, M.; Jin, F.; Nakamura, S. Activation of CO_2 by ionic liquid EMIM-BF4 in the electrochemical system: a theoretical study. *Physical Chemistry Chemical Physics* **2015**, *17* (36), 23521-23531.

17. Vasilyev, D. V.; Shyshkanov, S.; Shirzadi, E.; Katsyuba, S. A.; Nazeeruddin, M. K.; Dyson, P. J. Principal Descriptors of Ionic Liquid Co-catalysts for the Electrochemical Reduction of CO_2. *ACS Applied Energy Materials* **2020**, *3* (5), 4690-4698.

18. Dupont, J.; Simon, N. M.; Zanatta, M. The Nature of Carbon Dioxide in Bare Ionic Liquids. *ChemSusChem* **2020**, *13* (12), 3101-3109.

19. Sun, L. Y.; Ramesha, G. K.; Kamat, P. V.; Brennecke, J. F. Switching the Reaction Course of Electrochemical CO_2 Reduction with Ionic Liquids. *Langmuir* **2014**, *30* (21), 6302-6308.

20. Gu, L. Z., Y. Unexpected CO_2 Splitting Reactions To Form CO with N-Heterocyclic Carbenes as Organocatalysts and Aromatic Aldehydes as Oxygen Acceptors. *Journal of the American Chemical Society* **2010**, *132* (3), 914-915.

21. Noack, K.; Schulz, P. S.; Paape, N.; Kiefer, J.; Wasserscheid, P.; Leipertz, A. The role of the C2 position in interionic interactions of imidazolium based ionic liquids: a vibrational and NMR spectroscopic study. *Physical Chemistry Chemical Physics* **2010**, *12* (42), 14153-14161.

22. Whipple, D. T.; Kenis, P. J. A. Prospects of CO_2 Utilization via Direct Heterogeneous Electrochemical Reduction. *The Journal of Physical Chemistry Letters* **2010**, *1* (24), 3451-3458.

23. Kemna, A.; Braunschweig, B. Potential-Induced Adsorption and Structuring of Water at the Pt(111) Electrode Surface in Contact with an Ionic Liquid. *Journal of Physical Chemistry Letters* **2020**, *11* (17), 7116-7121.

24. König, M.; Vaes, J.; Klemm, E.; Pant, D. Solvents and Supporting Electrolytes in the Electrocatalytic Reduction of CO_2. *iScience* **2019**, *19*, 135-160.

25. Smith, A. M.; Lee, A. A.; Perkin, S. The Electrostatic Screening Length in Concentrated Electrolytes Increases with Concentration. *The Journal of Physical Chemistry Letters* **2016**, *7* (12), 2157-2163, Article.

26. Gebbie, M. A.; Valtiner, M.; Banquy, X.; Fox, E. T.; Henderson, W. A.; Israelachvili, J. N. Ionic liquids behave as dilute electrolyte solutions. *Proceedings of the National Academy of Sciences* **2013**, *110* (24), 9674-9679.

27. Gebbie, M. A.; Smith, A. M.; Dobbs, H. A.; Lee, A. A.; Warr, G. G.; Banquy, X.; Valtiner, M.; Rutland, M. W.; Israelachvili, J. N.; Perkin, S.; et al. Long range electrostatic forces in ionic liquids. *Chemical Communications* **2017**, *53* (7), 1214-1224.

28. Bazant, M. Z.; Storey, B. D.; Kornyshev, A. A. Double layer in ionic liquids: overscreening versus crowding. *Physical Review Letters* **2011**, *106* (4), 046102.

29. Kornyshev, A. A. Double-Layer in Ionic Liquids: Paradigm Change? *The Journal of Physical Chemistry B* **2007**, *111* (20), 5545-5557.

30. Lee, A. A.; Perez-Martinez, C. S.; Smith, A. M.; Perkin, S. Scaling Analysis of the Screening Length in Concentrated Electrolytes. *Physical Review Letters* **2017**, *119* (2), 026002.

31. de Souza, J. P.; Bazant, M. Z. Continuum Theory of Electrostatic Correlations at Charged Surfaces. *The Journal of Physical Chemistry C* **2020**, *124* (21), 11414-11421.

32. Gebbie, M. A.; Dobbs, H. A.; Valtiner, M.; Israelachvili, J. N. Long-range electrostatic screening in ionic liquids. *Proceedings of the National Academy of Sciences of the United States of America* **2015**, *112* (24), 7432-7437.

33. Han, M.; Kim, H.; Leal, C.; Negrito, M.; Batteas, J. D.; Espinosa-Marzal, R. M. Insight into the Electrical Double Layer of Ionic Liquids Revealed through Its Temporal Evolution. *Advanced Materials Interfaces* **2020**, *7* (24).

34. García Rey, N.; Dlott, D. D. Structural Transition in an Ionic Liquid Controls CO2 Electrochemical Reduction. *The Journal of Physical Chemistry C* **2015**, *119* (36), 20892-20899.

35. Lim, H.-K.; Kwon, Y.; Kim, H. S.; Jeon, J.; Kim, Y.-H.; Lim, J.-A.; Kim, B.-S.; Choi, J.; Kim, H. Insight into the Microenvironments of the Metal–Ionic Liquid Interface during Electrochemical CO_2 Reduction. *ACS Catalysis* **2018**, *8* (3), 2420-2427.

36. Hahn, C.; Jaramillo, T. F. Using Microenvironments to Control Reactivity in CO_2 Electrocatalysis. *Joule* **2020**, *4* (2), 292-294.

37. Hansen, K. U.; Jiao, F. Creating the right environment. *Nature Energy* **2021**, *6* (11), 1005-1006.

38. Kim, C.; Bui, J. C.; Luo, X.; Cooper, J. K.; Kusoglu, A.; Weber, A. Z.; Bell, A. T. Tailored catalyst microenvironments for CO_2 electroreduction to multicarbon products on copper using bilayer ionomer coatings. *Nature Energy* **2021**, *6* (11), 1026-1034.

39. Zhao, S.-F.; Horne, M.; Bond, A. M.; Zhang, J. Is the Imidazolium Cation a Unique Promoter for Electrocatalytic Reduction of Carbon Dioxide? *The Journal of Physical Chemistry C* **2016**, *120* (42), 23989-24001.

40. Tanner, E. E. L.; Batchelor-McAuley, C.; Compton, R. G. Carbon Dioxide Reduction in Room-Temperature Ionic Liquids: The Effect of the Choice of Electrode Material, Cation, and Anion. *The Journal of Physical Chemistry C* **2016**, *120* (46), 26442-26447.

41. Vasilyev, D. V.; Dyson, P. J. The Role of Organic Promoters in the Electroreduction of Carbon Dioxide. *ACS Catalysis* **2021**, *11* (3), 1392-1405.

42. Bard, A. J.; Faulkner, L. R. Electrochemical Methods: Fundamentals and Applications. 2 ed.; Wiley, 2001, p 23-28, 251-252, 417-418, 648-650.

43. Gu, J.; Liu, S.; Ni, W.; Ren, W.; Haussener, S.; Hu, X. Modulating electric field distribution by alkali cations for CO_2 electroreduction in strongly acidic medium. *Nature Catalysis* **2022**.

44. Monteiro, M. C. O.; Dattila, F.; Lopez, N.; Koper, M. T. M. The Role of Cation Acidity on the Competition between Hydrogen Evolution and CO2 Reduction on Gold Electrodes. *Journal of the American Chemical Society* **2022**, *144* (4), 1589-1602.

45. Marcandalli, G.; Goyal, A.; Koper, M. T. M. Electrolyte effects on the faradaic efficiency of CO_2 reduction to CO on a gold electrode. *ACS Catalysis* **2021**, *11* (9), 4936-4945.

46. Pavlishchuk, V. V.; Addison, A. W. Conversion constants for redox potentials measured versus different reference electrodes in acetonitrile solutions at 25°C. *Inorganica Chimica Acta* **1999**, *298*, 97-102.

47. Matsubara, Y.; Grills, D. C.; Kuwahara, Y. Thermodynamic Aspects of Electrocatalytic CO_2 Reduction in Acetonitrile and with an Ionic Liquid as Solvent or Electrolyte. *ACS Catalysis* **2015**, *5* (11), 6440-6452.

48. Santos, V. O.; Leite, I. R.; Brolo, A. G.; Rubim, J. C. The electrochemical reduction of CO_2 on a copper electrode in 1-n-butyl-3-methyl imidazolium tetrafluoroborate (BMI.BF4) monitored by surface-enhanced Raman scattering (SERS). *Journal of Raman Spectroscopy* **2016**, *47* (6), 674-680.

49. Michez, R.; Doneux, T.; Buess-Herman, C.; Luhmer, M. NMR Study of the Reductive Decomposition of [BMIm][NTf_2] at Gold Electrodes and Indirect Electrochemical Conversion of CO_2. *ChemPhyschem* **2017**, *18* (16), 2208-2216.

50. Monteiro, M. C. O.; Philips, M. F.; Schouten, K. J. P.; Koper, M. T. M. Efficiency and selectivity of CO_2 reduction to CO on gold gas diffusion electrodes in acidic media. *Nature Communications* **2021**, *12* (1), 4943.

51. Li, T.; Lees, E. W.; Goldman, M.; Salvatore, D. A.; Weekes, D. M.; Berlinguette, C. P. Electrolytic Conversion of Bicarbonate into CO in a Flow Cell. *Joule* **2019**, *3* (6), 1487-1497.

52. Rabinowitz, J. A.; Kanan, M. W. The future of low-temperature carbon dioxide electrolysis depends on solving one basic problem. *Nature Communications* **2020**, *11* (1), 5231.

53. Foley, J.; Korzeniewski, C.; Pons, S. Anodic and cathodic reactions in acetonitrile/tetra- n -butylammonium tetrafluoroborate: an electrochemical and infrared spectroelectrochemical study. *Canadian Journal of Chemistry* **1988**, *66* (1), 201-206.

54. Berto, T. C.; Zhang, L.; Hamers, R. J.; Berry, J. F. Electrolyte Dependence of CO_2 Electroreduction: Tetraalkylammonium Ions Are Not Electrocatalysts. *ACS Catalysis* **2014**, *5* (2), 703-707.

55. Dhumal, N. R.; Noack, K.; Kiefer, J.; Kim, H. J. Molecular Structure and Interactions in the Ionic Liquid 1-Ethyl-3-methylimidazolium Bis(Trifluoromethylsulfonyl)imide. *The Journal of Physical Chemistry A* **2014**, *118* (13), 2547-2557.

56. Sanchora, P.; Pandey, D. K.; Rana, D.; Materny, A.; Singh, D. K. Impact of Size and Electronegativity of Halide Anions on Hydrogen Bonds and Properties of 1-Ethyl-3-methylimidazolium-Based Ionic Liquids. *The Journal of Physical Chemistry A* **2019**, *123* (23), 4948-4963.

57. Santos, V. O.; Alves, M. B.; Carvalho, M. S.; Suarez, P. A. Z.; Rubim, J. C. Surface-Enhanced Raman Scattering at the Silver Electrode/Ionic Liquid ($BMIPF_6$) Interface. *The Journal of Physical Chemistry B* **2006**, *110* (41), 20379-20385.

58. Santos Jr, V. O.; Leite, I. R.; Brolo, A. G.; Rubim, J. C. The electrochemical reduction of CO_2 on a copper electrode in 1-n-butyl-3-methyl imidazolium tetrafluoroborate (BMI.BF4) monitored by surface-enhanced Raman scattering (SERS). *Journal of Raman Spectroscopy* **2016**, *47* (6), 674-680.

59. Siddiqui, S. A.; Dubey, K. D. Can the local electric field be a descriptor of catalytic activity? A case study on chorismate mutase. *Physical Chemistry Chemical Physics* **2021**, *24*, 1974-1981.

60. Léonard, N. G.; Dhaoui, R.; Chantarojsiri, T.; Yang, J. Y. Electric Fields in Catalysis: From Enzymes to Molecular Catalysts. *ACS Catalysis* **2021**, *11* (17), 10923-10932.

61. Resasco, J.; Chen, L. D.; Clark, E.; Tsai, C.; Hahn, C.; Jaramillo, T. F.; Chan, K.; Bell, A. T. Promoter Effects of Alkali Metal Cations on the Electrochemical Reduction of Carbon Dioxide. *Journal of the American Chemical Society* **2017**, *139* (32), 11277-11287.

62. Lee, G.; Li, Y. C.; Kim, J.-Y.; Peng, T.; Nam, D.-H.; Sedighian Rasouli, A.; Li, F.; Luo, M.; Ip, A. H.; Joo, Y.-C.; et al. Electrochemical upgrade of CO_2 from amine capture solution. *Nature Energy* **2020**, *6* (1), 46-53.

63. Fedorov, M. V.; Kornyshev, A. A. Ionic liquids at electrified interfaces. *Chemical Reviews* **2014**, *114* (5), 2978-3036.

64. Rudnev, A. V.; Zhumaev, U. E.; Kuzume, A.; Vesztergom, S.; Furrer, J.; Broekmann, P.; Wandlowski, T. The promoting effect of water on the electroreduction of CO_2 in acetonitrile. *Electrochimica Acta* **2016**, *189*, 38-44.

65. Figueiredo, M. C.; Ledezma-Yanez, I.; Koper, M. T. M. In Situ Spectroscopic Study of CO_2 Electroreduction at Copper Electrodes in Acetonitrile. *ACS Catalysis* **2016**, *6* (4), 2382-2392.

66. Chae, K. J.; Choi, M.; Ajayi, F. F.; Park, W.; Chang, I. S.; Kim, I. S. Mass Transport through a Proton Exchange Membrane (Nafion) in Microbial Fuel Cells. *Energy and Fuels* **2008**, *22* (1), 169-176.

67. Sheng, H.; Hermes, E. D.; Yang, X.; Ying, D.; Janes, A. N.; Li, W.; Schmidt, J. R.; Jin, S. Electrocatalytic Production of H_2O_2 by Selective Oxygen Reduction Using Earth-Abundant Cobalt Pyrite (CoS_2). *ACS Catalysis* **2019**, *9* (9), 8433-8442.

68. Han, N.; Wang, Y.; Yang, H.; Deng, J.; Wu, J.; Li, Y.; Li, Y. Ultrathin bismuth nanosheets from in situ topotactic transformation for selective electrocatalytic CO_2 reduction to formate. *Nature Communications* **2018**, *9* (1), 1320.

69. Agnihotri, S.; Mukherji, S.; Mukherji, S. Size-controlled silver nanoparticles synthesized over the range 5–100 nm using the same protocol and their antibacterial efficacy. *RSC Advances* **2014**, *4* (8), 3974-3983.